

Journal of Water and Wastewater, Vol. 32, No. 5, pp: 1-11

# Adsorption of Alizarin Red S Dye on Raw Endoskeleton Nanopowder of Cuttlefish (*Sepia Pharaonis*) from Water Solutions: Mechanism, Kinetics and Equilibrium Modeling

N. Rahbar<sup>1</sup>, K. Tabatabaie<sup>2</sup>, Z. Ramezani<sup>3</sup>

1. Prof., Marine Pharmaceutical Science Research Center, Ahvaz Jundishapur University of Medical Sciences, Ahvaz, Iran  
(Corresponding Author) n\_rahbar2010@ajums.ac.ir
2. Pharm. D., Student Research Committee, Ahvaz Jundishapur University of Medical Sciences, Ahvaz, Iran
3. Prof., Nanotechnology Research Center, Ahvaz Jundishapur University of Medical Sciences, Ahvaz, Iran

(Received Sep. 14, 2020 Accepted Nov. 15, 2020)

## To cite this article:

Rahbar, N., Tabatabaie, K., Ramezani, Z. 2022. "Adsorption of alizarin red S dye on raw endoskeleton nanopowder of cuttlefish (*Sepia Pharaonis*) from water solutions: mechanism, kinetics and equilibrium modeling" Journal of Water and Wastewater, 32(5), 1-11. Doi: 10.22093/wwj.2020.248031.3065.

## Abstract

The potential of the raw cuttlebone nano-powder (CBNP), a biomass waste, as a novel and nontoxic adsorbent for the adsorption of Alizarin Red S (ARS) from water solutions was investigated. To achieve the highest efficiency for the removal of ARS, some affecting factors were optimized. Common techniques (FTIR, FESEM, EDX and XRF) were used to characterize the physicochemical features of the adsorbent. Various kinetic and isotherm models were used to obtain the useful information about the adsorption mechanism of the dye onto the adsorbent. The maximum dye removal efficiency was obtained with the adsorbent amount of 500 mg (in 50 mL) and initial pH of 2 in 10 min for 20 mg/L ARS solution. Under these optimum conditions the complete removal of ARS was obtained while the maximum adsorption capacity was 38.51 mg/g. The well fitness of pseudo-second order kinetic model in the adsorption process was proved by kinetic studies. According to the obtained results, Freundlich isotherm model can suitably describe the adsorption of ARS on the sorbent. The achieved results from this study showed the excellent capability of CBNP for the adsorption of ARS.

**Keywords:** Alizarin Red S, *Sepia Pharaonis*, Cuttlebone, Removal, Adsorption.

## 1. Introduction

Dyes are discharged into the natural streams from various industrial activities such as textile finishing, dye manufacturing, food coloring, cosmetics, paper, and carpet industries. Among them the textile industry produces high volume of waste water with toxic

composition. Textile effluents have strong colors because of incomplete dye fixation process on fibers which vary from 5% to 80% of the initial amount of dye used (Gomesa et al., 2010). The toxicity (carcinogen or mutagenic effects) and accumulation of dye waste waters



can present serious environmental problems. Generally, the synthetic dyes are categorized based on their chemical structures including triphenylmethane, anthraquinone, azo, indigoid, sulfur, and phthalocyanine derivatives (Mishra et al., 2010).

Nowadays, great interest is focused on the removal of hazardous dyestuff from industrial effluents through adsorption on a solid phase (Salama et al., 2015, Shen et al., 2011, Mishra et al., 2010, Al-Ghouti et al., 2009, Tan et al., 2012, Nopkhuntod et al., 2012, Demarchi et al., 2013). The use of low cost sorbents for water treatment has become an alternative to the expensive ones such as membranes, ion exchangers and carbon materials. Persistent efforts have recently been made to build up highly effective, low cost, ecofriendly and locally available adsorbents. Low-cost adsorbents are natural materials such as agricultural waste and by-products of industries (such as fishery waste) which can be exploited as adsorbents without or after some minor treatment (Gupta, 2009; Rangabhashiyam et al., 2013; Allen and Koumanova, 2005). Cuttlefish bone (endoskeleton of *Sepia*) or cuttlebone is the cuttlefish processing waste in fishery industry. It also exists naturally in beaches where cuttlefish live. It has an oblong oval shape (10-25 cm long and 4-7.5 cm broad) with a chitinous coat. Basically, the main constituents of the cuttlebone are calcium carbonate and organic matter.

Alizarin red S or alizarin red sulfonate (ARS) is sodium salt of 1, 2-dihydroxy-9, 10-anthraquinonesulfonic acid and belongs to the anthraquinone class of dyes which is derived from the roots of plants of the madder genus. This dye has been extensively used as an important dye since ancient times in textile industry (Rehman et al., 2011). A Mordant dye such as ARS with functional groups like hydroxyl, carbonyl, and sulfonate (Fig. 1) is capable to react strongly with metals to form salt or complex structures (Moriguchi et al., 2003). For this reason, ARS can be used for identification of calcium in tissue sections (Puchtler et al., 1969).

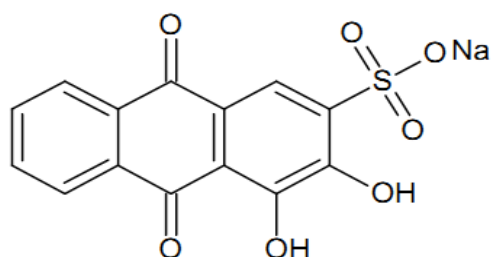


Fig. 1. The chemical structure of Alizarin Red S

So far, tremendous effort has been made to remove this dye from water and industrial effluents (Adlnasab et al., 2017; Embaby et al., 2018; Kamarehie et al., 2018; Liang et al., 2018; Yang et al., 2018; Zhang et al., 2019; Liu et al., 2020; Fan et al., 2012; Lemlikchi et al., 2014; Zolgharnein et al., 2014; Gholivand et al., 2015; Ghaedi

et al., 2012). A few published data are available for the removal of ARS by low cost and nano-sized untreated biomass adsorbents. In these studies, adsorbents such as mentha waste and mustard husk have been used (Gautam et al., 2013; Ahmad and Kumar, 2008).

The main goal of this study is to exploit cuttlefish bone as a low cost resource and waste material for the treatment of dye wastewater by inexpensive technique. In addition, the use of nano-sized adsorbents (<100 nm) with high active sites and large specific surface area have exhibited better performance than the conventional adsorbents (Zhang et al., 2019). Therefore, in the present work cuttlebone nano-powder (CBNP) was used for the first time as a biomass for ARS removal. The sorption behavior of ARS onto the untreated powdered cuttlebone (extent of adsorption, isotherm, and kinetic mechanisms) and the optimized experimental conditions were investigated.

## 2. Experimental

### 2.1. Materials

ARS was provided from Merck (Germany). Cuttlebones were obtained from Nakhiloo Island near the North coast of Persian Gulf in Bushehr Province, Iran, in September 2019. The solvents including acetone ( $\text{CH}_3\text{OCH}_3$ ) and ethanol ( $\text{C}_2\text{H}_5\text{OH}$ ) were supplied by Samchun Chemicals Company. Sodium hydroxide (NaOH), Hydrochloric acid (HCl), and acetic acid ( $\text{CH}_3\text{COOH}$ ) were obtained from Merck. All the reagents and solvents were analytical grade and deionized water was used through out the experiments.

### 2.2. Preparation of cuttlebone nanopowder

Before use, the cuttlebone was brushed to remove any adhered materials. After that, it was rinsed with deionized water and dried for 24 h at 60 °C. Afterwards, it was thoroughly ground in a lab mortar and sieved using a 100 mesh sieve. The resulting nanopowder was kept in a desiccator.

### 2.3. Characterization of the cuttlefish bone nanopowder

Fourier transform infrared<sup>1</sup> spectra of CBNP and CBNP/ARS were recorded using a Bruker spectrometer (model Tensor 27, Germany), in the scanning range of 400-4000  $\text{cm}^{-1}$ . Field emission scanning electron microscopy<sup>2</sup> and energy dispersive x-ray spectroscopy<sup>3</sup> were used to show the dimensions, morphology and composition of CBNP (Nanowizard II, Germany). Elemental analysis of CBNP was obtained by Oxford (model ED 2000) x-ray fluorescence<sup>4</sup> instrument.

<sup>1</sup> Fourier Transform Infrared (FTIR)

<sup>2</sup> Field Emission Scanning Electron Microscopy (FESEM)

<sup>3</sup> Energy Dispersive X-Ray Spectroscopy (EDX)

<sup>4</sup> X-Ray Fluorescence (XRF)

## 2.4. Batch adsorption experiment

The batch mode experiments were carried out by mixing 50 mL of ARS solutions (1-400 mg/L) and the amounts of CBNP in the range of 25.0-1000.0 mg. HCl and NaOH solutions were used to adjust the initial pH of the solution to the definite value (2-10).

The solution samples were stirred (at 25 °C and 500 rpm) at the fixed intervals of 2-120 min, and then centrifuged for 10 min at 4000 rpm. After separation of the solution from sedimented CBNP, the dye concentration was measured using a Jasco 7800 spectrophotometer. The determinations were accomplished in 536 nm ( $\lambda_{\max}$  of ARS). The removal efficiency of ARS (R%) was assessed using Eq. (1)

$$R\% = \frac{C_0 - C_t}{C_0} \times 100 \quad (1)$$

where

$C_0$  and  $C_t$  are the initial concentration of ARS (mg/L) at the beginning and the time  $t$ , respectively. CBNP loading capacity at the equilibrium ( $q_e$ ) was determined as

$$q_e = \frac{(C_0 - C_e) \times V}{W} \quad (2)$$

where

$V$  and  $W$  are the solution volume (L) and the adsorbent amount (g), respectively. The influences of the experimental factors on the adsorption capacity of CBNP were investigated. All experiments were repeated 3 times and the result was presented as an average. The photographs of cuttlebone, raw CBNP and CBNP after the adsorption of ARS are shown in Fig. 2.

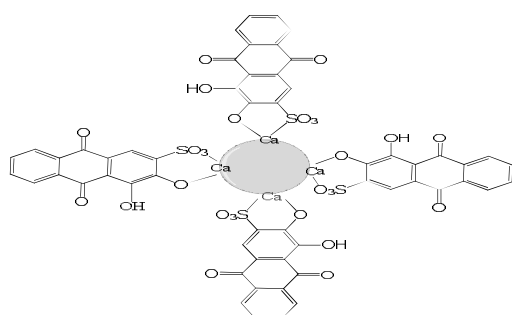


**Fig. 2.** The proposed structure for ARS adsorbed on CBNP

## 3. Results and Discussion

### 3.1. CBNP characteristics

The FTIR spectra of CBNP before and after ARS adsorption are shown in Figs. 3a and 3b. The major band at 1467  $\text{cm}^{-1}$  and the sharp band at 854  $\text{cm}^{-1}$  are related to C-O the Ca-O bonds in carbonate constituent of

CBNP, respectively (Fig. 4a). Furthermore, the broad band of -OH and -NH and the reference absorption band of chitin are seen at 3200-3500  $\text{cm}^{-1}$  and 2900  $\text{cm}^{-1}$ , respectively. The lower absorption bands at 610-707  $\text{cm}^{-1}$  might be caused by chitinous constituent of CBNP. The representative absorption bands of ARS molecule are appeared at 1160  $\text{cm}^{-1}$  (-SO<sub>3</sub>), 1670-1700  $\text{cm}^{-1}$  (C-O), 1462  $\text{cm}^{-1}$  (aromatic ring) and 1338 at  $\text{cm}^{-1}$  (-OH). As shown in Fig. 4b, these bands may overlap by the broad bands of C-O (in CBNP) at 1467  $\text{cm}^{-1}$ . However the absorption band appeared at 1627  $\text{cm}^{-1}$  may be attributed to the C=O functional group in ARS (Moriguchi et al., 2003; Puchtler et al., 1969; Zolgharnein et al., 2014). The results obtained from XRF analysis are shown in Fig. 5. As seen, the data are consistent to FTIR achievements, showing that Ca (as CaO or CaCO<sub>3</sub>) is the main constituent of the adsorbent. The FESEM image and EDX spectrum of CBNP is presented in Fig. 6. As can be seen from Fig. 6a, CBNP particles with spherical shapes have diameters about 22-24 nm, representing large surface area of the adsorbent and large absorption sites for dye molecules. Moreover, the EDX spectrum of the adsorbent confirmed the XRF data (Fig. 6b).

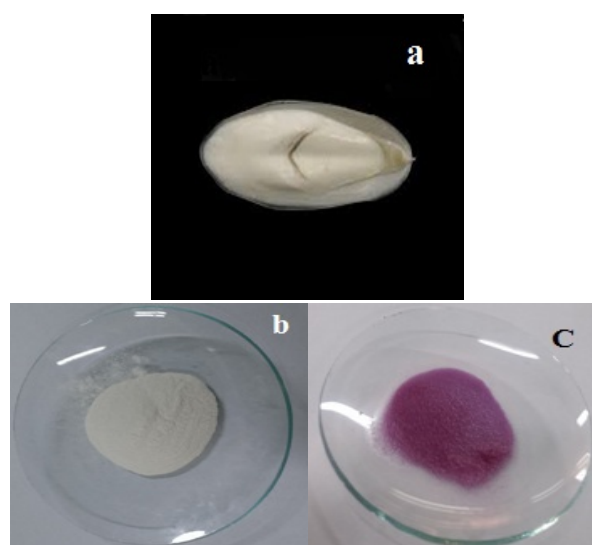


**Fig. 3.** Cuttlebone a) raw CBNP, b) CBNP after adsorption of ARS and c) at pH 8

### 3.2. Influence of solution pH

The pH of the solution can be an important parameter affecting the dye adsorption on the adsorbent. This dependence of the dye removal on the pH value is due to both the dye and the adsorbent chemistry. To evaluate the effect of this parameter on the removal process, 50 mL of ARS solutions (10 mg/L of the dye) with pH in the range of 2-10 were subjected to the adsorption process. The results are shown in Fig. 7, indicating that maximum removal for ARS is achieved at pH 2. It is



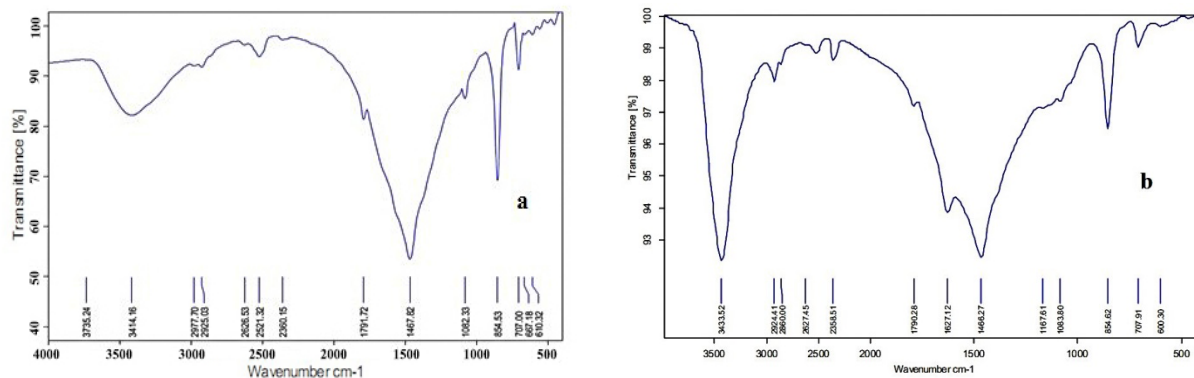


Fig. 4. FTIR spectra of: a) CBNP b) ARS-CBNP

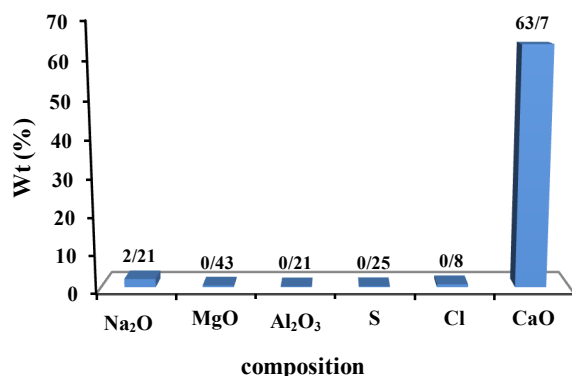


Fig. 5. Data obtained from X-Ray Fluorescence elemental analysis

worthy to mention that as stated in section 3.1, the main constituent of CBNP is calcium carbonate and it is predictable that when it is agitated with the ARS solution, the increase in pH is observed. By adjustment of the initial pH of the dye solutions in the range of 2-10, the final pH values became 8.6-9.3 after agitation in the presence of CBNP. In these final pHs, the color of ARS changed to pink and therefore, residual dye concentration in the solution was determined in  $\lambda_{\max} = 536$  nm. Regarding the pKa values of ARS ( $\text{pK}(2\text{-OH}) = 5.49$  and  $\text{pK}(1\text{-OH}) = 10.85$ ), ARSH<sup>-</sup> is predominant in the solution at the pH range of 8.6-9.3 (Lemlikchi et al., 2014). Obtaining the maximum percentage of ARS removal in pH 2 (final pH of 8.6) suggests that the adsorption of the dye can be ascribed to the formation of Ca-ARS salt via 2-O<sup>-</sup> and sulfonate group, because in this pH almost all ARS molecules exist in ARSH<sup>-</sup> form and 1-OH group is not in the ionized form (Fig. 1).

As shown in Fig. 7, at the higher pHs (4-10), the adsorption of ARS was decreased to some extent (removal percent of about 88-90), which might be due to the insolubility of calcium carbonate in these pHs and unavailability of Ca(II) ions. Therefore, it can be concluded that the calcium ions can react with ARS to produce an insoluble salt in the surface of CBNP,

properly (Puchtler et al., 1969). Based on the previous studies, ARS can be adsorbed on fluorite, calcite, and apatite minerals. In all cases it has been assumed that ARS molecule reacted with calcium sites at the mineral surface. Moreover, ARS has been used as histochemical stain for coloring calcium deposits in tissues, for a long time (Holmgren et al., 1999; Lemlikchi et al., 2014; Puchtler et al., 1969).

The mechanism of ARS adsorption on hydroxyapatite (HAP) has been reported previously (Moriguchi et al., 2003). In this report, a major mechanism of salt formation between ARS (1- and 2-O<sup>-</sup>) and Ca<sup>2+</sup> on HAP has been proposed. There are some similarities between our findings and the other researches mentioned above.

However, in the case of CBNP, it seems that existence of calcium carbonate and its solubility in moderate pHs causes another mechanism for ARS adsorption participating electrostatic forces (between Ca(II) and ARS 2-O<sup>-</sup> group) and ion exchange mechanism (between sulfonate group and bicarbonate ion). Consequently, here we propose the structure that is shown in Fig. 2.

### 3.3. The adsorbent amount effect

The dosage of adsorbent is another important factor to obtain quantitative removal. Therefore, to achieve the maximum adsorption of the dye, CBNP amount effect (25-1000 g) was investigated for 50 mL of the solutions containing 10 mg/L of ARS at initial pH 2. As illustrated in Fig. 8, nearly 100% removal was achieved when the amount of CBNP was 500 mg. The enhancement in removal efficiency with adsorbent amount might be related to the increased surface of the adsorbent and the existence of more adsorption sites. By increasing CBNP amount, more adsorption sites are available for adsorption because of the increase in surface area of adsorbent. Therefore, the dye can penetrate easier to the adsorption sites (Liang et al., 2018). Based on the results, a CBNP amount of 0.5 g was chosen for use in further experiments.

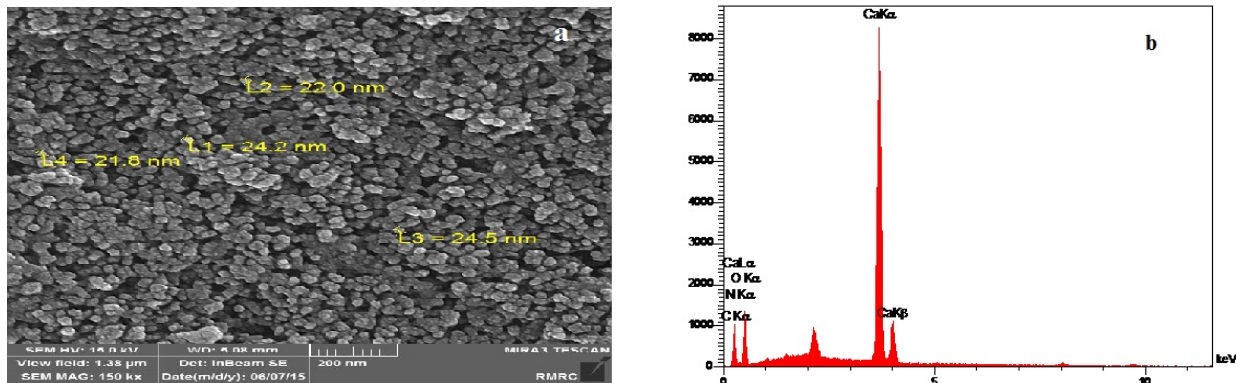


Fig. 6. a) FESEM photograph and b) EDX spectrum of CBNP

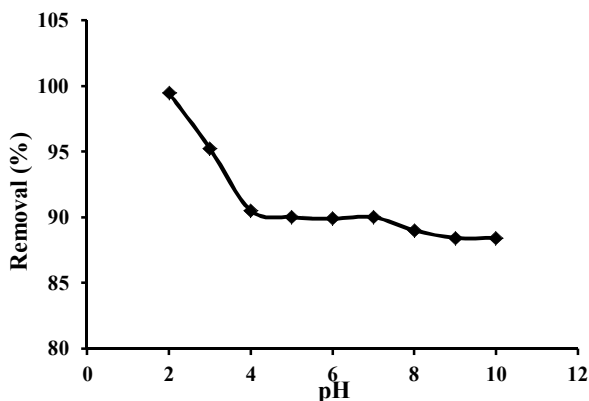


Fig. 7. Effect of pH on the adsorption of ARS on CBNP (conditions: 50 mL of ARS solution, 10 mg/L; CBNP amount, 500 mg; reaction time, 10 min; agitation rate, 500 rpm at 25 °C)

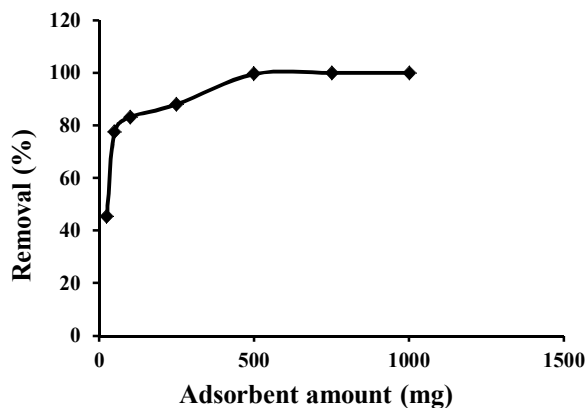


Fig. 8. Effect of the amount of adsorbent on the adsorption of ARS on CBNP (conditions: 50 mL of ARS solution, 10 mg/L, pH=2, reaction time, 10 min; agitation rate, 500 rpm at 25 °C)

### 3.4. Influence of contact time and Kinetic studies

The effect of contact time on the adsorption process was evaluated by using the ARS solution (10 mg/L) with 500 mg CBNP, at initial pH 2 and different time intervals (2 min-2 hours). The illustrated results in Fig. 9 reveal that

the adsorption rate is high for ARS and the examined dye adsorption reaches the equilibrium with about 100% removal in 10 min. Such a rapid adsorption indicates the strong attraction between dye molecules (as discussed before) and CBNP via chemical binding or electrostatic attraction. Kinetic of bio-sorption is the principal characteristic to determine the sorption efficiency. The adsorption rate of the target is controlled by the residence time in the solid-liquid interface. Therefore, three kinetic models, namely pseudo first-order, pseudo second-order and intra-particle diffusion were exploited to elucidate the kinetic mechanism of adsorption process (Jiang et al., 2013). The correlation coefficients values ( $R^2$ ) were used to select the best model fitted to the experimental data. The equations for the linear form of pseudo first-order (Eq. 3), pseudo second-order (Eq. 4), and intra-particle diffusion (Eq. 5) kinetic models are:

$$\frac{1}{q_t} = \frac{k_1}{q_e t} + \frac{1}{q_e} \quad (3)$$

$$\frac{t}{q_t} = \frac{1}{k_2 q_e^2} + \frac{t}{q_e} \quad (4)$$

$$q_t = k_{ip} \times t^{1/2} + C \quad (5)$$

where

$q_e$  and  $q_t$  (mg/g) are the adsorption capacities in equilibrium and time  $t$  (min). In addition,  $k_1$  ( $\text{min}^{-1}$ ),  $k_2$  ( $\text{g mg}^{-1} \text{min}^{-1}$ ), and  $k_{ip}$  ( $\text{mg/g min}^{1/2}$ ) are pseudo first-order, pseudo-second-order, and intra-particle diffusion rate constants, respectively. The linear graphs of three kinetic models were plotted (Figs. 8a-c) and based on the measured data the pseudo second-order model was the better model for explanation of the results.  $t/q_t$  plot versus  $t$  for the target dye yielded very good straight line and correlation coefficient ( $> 0.999$ ) and therefore, this kinetic model suitably described the bio-sorption of ARS onto CBNP (Fig. 10b). The values for the parameters of kinetic models are presented in Table 1.

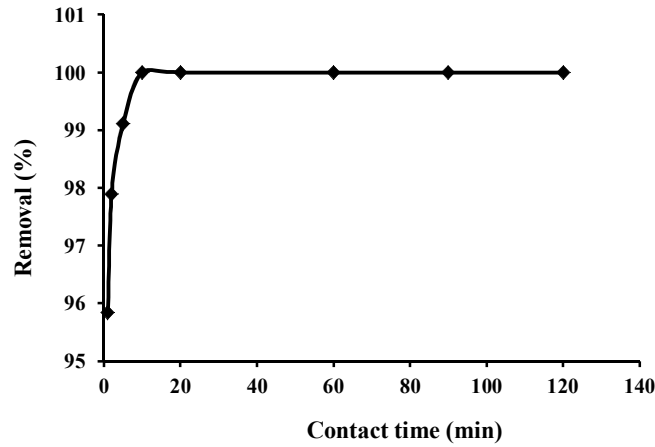


Fig. 9. Effect of the contact time on the adsorption of ARS on CBNP (conditions: 50 mL of ARS solution, 10 mg/L; pH=2; CBNP amount, 500 mg; agitation rate, 500 rpm at 25°C)

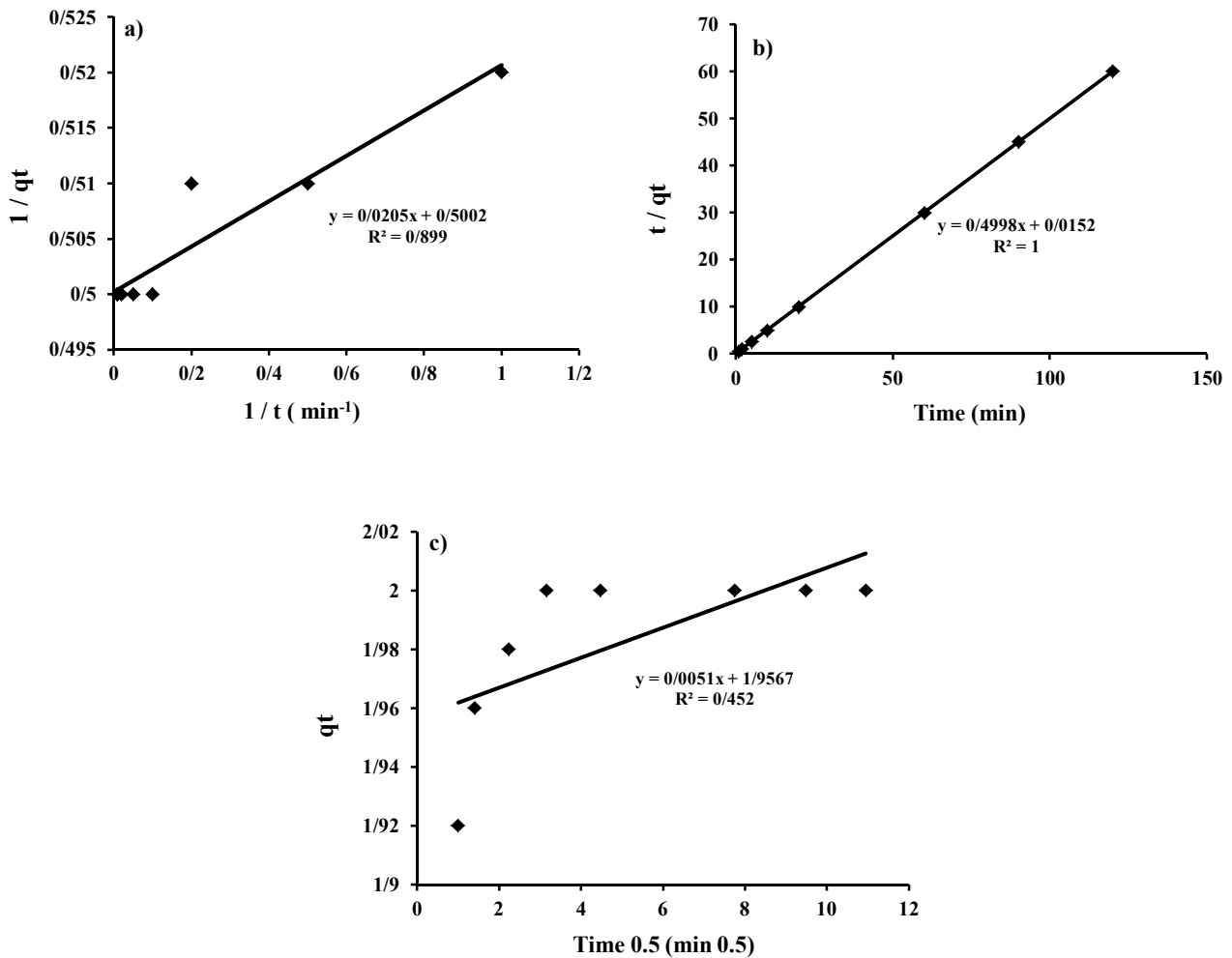


Fig. 10. a) Pseudo first-order, b) pseudo second-order and c) intra-particle diffusion kinetic plots for the adsorption of ARS on CBNP

**Table 1.** The values for the parameters of three kinetic models of ARS adsorption on CBNP

Kinetic models	Parameters		
Pseudo-first-order	$q_{e, Cal}$ (mg/g) 1.99	$k_1$ ( $\text{min}^{-1}$ ) 0.041	$R^2$ 0.899
Pseudo-second-order	$q_{e, Cal}$ (mg/g) 2.00	$K_2$ ( $\text{g mg}^{-1} \text{min}^{-1}$ ) 16.45	$R^2$ 1
Intra-particle diffusion	$k_{ip}$ ( $\text{mg/g min}^{1/2}$ ) 0.0051	C 1.9567	$R^2$ 0.452

### 3.5. Effect of concentration of ARS on removal and their adsorption isotherms

#### 3.5.1. Influence of ARS concentration and adsorption isotherms

The influence of initial concentration of ARS (1-500 mg/L) on the adsorption by CBNP under optimized conditions is shown in Fig. 11. As seen, ARS is adsorbed quantitatively by CBNP up to 20 mg/L, while in higher concentrations the removal efficiency decreases slowly. The decrease of removal percentage in concentrations higher than 20 mg/L is owing to the limited surface area and available adsorption sites of 500 mg CBNP (Liang et al., 2018). On the other hand, an increase in initial concentration of ARS can enhance the adsorption uptake of the dye, which might be due to the increase in the driving force of the concentration gradient. Therefore, for 20 mg/L of ARS solution removal percentage was found to be 100% (equivalent to 1 mg of ARS), while this value for that of 500 mg/L was 77% (equivalent to 19.25 mg of ARS) (Gautam, et al., 2013).

Adsorption isotherms of ARS were studied with the concentrations of the dye between 1-500 mg/L. Langmuir (Eq. 6) and Freundlich (Eq. 7) isotherm models were used to describe the adsorption equilibrium data

$$\frac{C_e}{q_e} = \frac{C_e}{q_m} + \frac{1}{K_L q_m} \quad (6)$$

$$\text{Log } q_e = \log K_F + \frac{1}{n} \log C_e \quad (7)$$

where

$C_e$  (mg/L),  $q_e$  (mg/g), and  $q_m$  (mg/g) are the equilibrium concentration of ARS, the amount of the dye adsorbed on CBNP at equilibrium conditions, and the maximum adsorption capacity of CBNP, respectively.  $K_L$  (L mg/g) and  $K_F$  (mg/g) are Langmuir and Freundlich constants. Finally,  $1/n$  (L/mg) is related to the intensity of adsorption ( $n > 1$  is favorable) (Rahbar et al., 2014).  $R_L$  is called the separation factor and indicates the degree of suitability of the adsorbent toward the target and can be assessed by using  $K_L$  (Eq. 8).

$$R_L = \frac{1}{1 + C_0 K_L} \quad (8)$$

The magnitude of  $R_L$  is used to define the adsorption process:  $R_L > 1.0$  (unsuitable);  $R_L = 1$  (linear),  $0 < R_L < 1$  (suitable), and  $R_L = 0$  (irreversible) (Monier and Abdel-Latif, 2012).

Theoretically, according to Langmuir isotherm all adsorption sites on the adsorbent are energetically identical and homogeneous. Furthermore, in this isotherm, a monolayer adsorption is occurred on the surface of adsorbent. As opposed to Langmuir isotherm, Freundlich isotherm describes the molecule adsorption on energetically heterogeneous surface and the molecule adsorption is not limited to the formation of monolayer (Monier and Abdel-Latif, 2012). The linear curves of Freundlich and Langmuir isotherms were plotted for ARS adsorption and the parameters related to these isotherms are given in Table 2. As the results indicate, Freundlich model can better describe the adsorption of ARS on heterogeneous surface of CBNP.

#### 3.6. Desorption studies

Desorption characteristics of the adsorbent are examined using 5 mL of different solvents including HCl 0.1-1 mol/L, NaOH 0.1-1 mol/L, acetone, ethanol, and acetic acid 0.1-1 mol/L. Also, various mixtures of acetone and ethanol (30:70, 50:50 and 70:30 v/v) were tested in order to recover the dye from CBNP. The maximum desorption of the saturated adsorbent was achieved when 1 mol/L acetic acid solution was used with 96% ARS recovery. The results indicated that in moderate acidic condition provided by acetic acid the salt formation reaction was not favorable, possibly due to the existence of ARS molecules in  $\text{ARSH}_2$  form.

#### 3.7. Comparison of CBNP with the other Adsorbents

The maximum adsorption capacity of CBNP was compared with the other reported adsorbents for the removal of ARS and the results are shown in Table 3. The  $q_m$  of the present adsorbent is found to be comparable or better than the other sorbents in most cases. Furthermore, many of the adsorbents presented in the table are synthesized in a complex manner with high cost. Whereas CBNP is thoroughly environmental compatible and it is a natural, nontoxic and cost effective source.

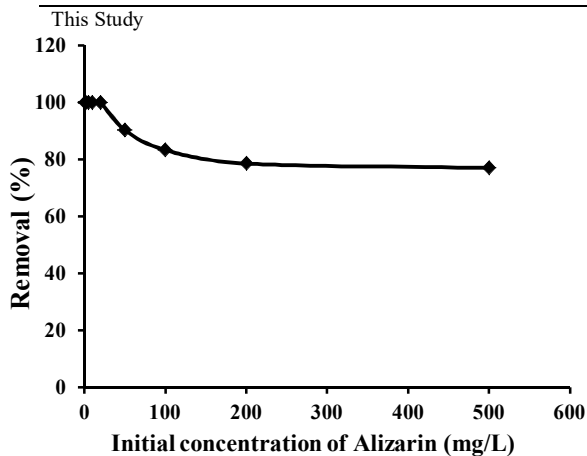


**Table 2.** Adsorption isotherms parameters for ARS adsorption on CBNP

Isotherm model	$q_{\max}$ (cal) (mg/g)	$q_{\max}$ (exp) (mg/g)	$K_L$	$K_F$	$R_L$	n	$R^2$
Langmuir	71.43	38.51	0.009	-	0.85	-	0.671
Freundlich	-	38.51	-	1.43	-	1.49	0.978

**Table 3.** The maximum adsorption capacities for ARS using adsorbents reported in the literature

Adsorbent	$q_m$ (mg/g)	Reference
Mentha waste	95.59	(Ahmad and Kumar, 2008)
Magnetic chitosan	43.08	(Fan et al., 2012)
Activated carbon	85.16	(Ghaedi et al., 2012)
Mustard husk	0.51	(Gautam et al., 2013)
Nano $\gamma$ -alumina	54.40	(Zolgharnein et al., 2014)
Polypyrrole-coated magnetic nanoparticles	116.3	(Gholivand et al., 2015)
Powdered activated carbon	24.5	(Kamarehie et al., 2018)
Treated powdered activated carbon	57.80	(Kamarehie et al., 2018)
Powdered activated carbon / $\gamma$ - $Fe_2O_3$	112.56	(Kamarehie et al., 2018)
Ni $Fe_2O_4$ /polyaniline magnetic composite	186	(Liang et al., 2018)
Pentaerythritol modified multi-walled carbon nanotube	257.73	(Yang et al., 2018)
Polyethyleneimine functionalized magnetic carbon nanotubes	196.08	(Zhang et al., 2019)
Zirconium (IV)-loaded chitosan/ $Fe_3O_4$ /graphene oxide	231.0	(Liu et al., 2020)
3-aminopropyltriethoxysilane grafted vermiculite	18.2	(Ali et al., 2020)
3-aminopropyltriethoxysilane grafted silica	59.8	(Ali et al., 2020)
CBNP	71.43	This work

**Fig. 11.** Effect of ARS concentration on the adsorption of ARS on CBNP (conditions: volume of ARS solution, 50 mL; pH=2; CBNP amount, 500 mg; agitation rate, 500 rpm at 25 °C)

showed that this adsorbent with large capacity of 71.43 mg/g for ARS adsorption is comparable and better than the other adsorbents in some cases (Table 3).

Although in some cases other adsorbents have shown better performance, it should be noted that this natural and non-toxic adsorbent is used without any special pretreatment and its use is quite cost-effective. In addition, the adsorption isotherms for the dye being investigated can be described well by Freundlich model.

The mechanism of the dye uptake by CBNP was extensively investigated and it was confirmed that the main mechanism is salt formation between Ca(II) and ionic groups in ARS ( $2-O^-$  and  $-SO_3^-$ ). Moreover, the particle size of CBNP in nanometer range explains the excellent capability of this sorbent for the adsorption of ARS. These results can open new fields for the future applications of CBNP in the removal of anthraquinone, anionic, and acidic dyes from wastewaters and dyeing effluents.

#### 4. Conclusions

In the present study a new biomass waste was introduced as a sorbent material for the effective removal of ARS from water bodies. Rapid adsorption (< 10 min), environment compatibility, and low cost are the main advantages of this sorbent. The experimental results

#### 5. Acknowledgements

The authors gratefully acknowledge the financial support provided by the Research Council of Ahvaz Jundishapur University of Medical Sciences under grant number GP93070. This paper is extracted from Dr. Tabatabaie's thesis.

## References

- Adlnasab, L., Shabaniyan, M., Ezoddin, M. & Maghsodi, A. 2017. Amine rich functionalized mesoporous silica for the effective removal of alizarin yellow and phenol red dyes from waste waters based on response surface methodology. *Materials Science and Engineering: B*, 226, 188-198.
- Ahmad, R. & Kumar, R. 2008. Comparative adsorption study for the removal of Alizarin Red S and patent Blue VF by using mentha waste. *Current World Environment*, 3, 261-268.
- Al-Ghouti, M. A., Al-Degs, Y. S., Khraisheh, M. A., Ahmad, M. N. & Allen, S. J. 2009. Mechanisms and chemistry of dye adsorption on manganese oxides-modified diatomite. *Journal of Environmental Management*, 90, 3520-3527.
- Ali, N., Ali, F., Ullah, I., Ali, Z., Duclaux, L., Reinert, L., et al. 2020. Organically modified micron-sized vermiculite and silica for efficient removal of Alizarin Red S dye pollutant from aqueous solution. *Environmental Technology and Innovation*, 19, 101001.
- Allen, S. J. & Koumanova, B. 2005. Decolourisation of water/wastewater using adsorption (review). *Journal of the University of Chemical Technology and Metallurgy*, 40, 175-192.
- Demarchi, C. A., Campos, M. & Rodrigues, C. A. 2013. Adsorption of textile dye Reactive Red 120 by the chitosan-Fe(III)-crosslinked: batch and fixed-bed studies. *Journal of Environmental Chemical Engineering*, 1, 1350-1358.
- Embaby, M. S., Elwany, S. D., Setyaningsih, W. & Saber, M. R. 2018. The adsorptive properties of UiO-66 towards organic dyes: a record adsorption capacity for the anionic dye Alizarin Red S. *Chinese Journal of Chemical Engineering*, 26, 731-739.
- Fan, L., Zhang, Y., Li, X., Luo, C., Lu, F. & Qiu, H. 2012. Removal of Alizarin Red from water environment using magnetic chitosan with Alizarin Red as imprinted molecules. *Colloids Surfaces B, Biointerfaces*, 91, 250-257.
- Gautam, R. K., Mudhoo, A. & Chattopadhyaya, M. C. 2013. Kinetic, equilibrium, thermodynamic studies and spectroscopic analysis of Alizarin Red S removal by mustard husk. *Journal of Environmental Chemical Engineering*, 1, 1283-1291.
- Ghaedi, M., Najibi, A., Hossainian, H., Shokrollahi, A. & Soylak, M. 2012. Kinetic and equilibrium study of Alizarin Red S removal by activated carbon. *Toxicological and Environmental Chemistry*, 94, 40-48.
- Gholivand, M. B., Yamini, Y., Dayeni, M., Seidi, S. & Tahmasebi, E. 2015. Adsorptive removal of Alizarin Red-S and Alizarin Yellow GG from aqueous solutions using polypyrrole-coated magnetic nanoparticles. *Journal of Environmental Chemical Engineering*, 3, 529-540.
- Gomesa, A. C., Nunesa, J. C. & Simõesa, R. M. S. 2010. Determination of fast ozone oxidation rate for textile dyes by using a continuous quench-flow system. *Journal of Hazardous Materials*, 178, 57-65.
- Gupta, V. K. 2009. Application of low-cost adsorbents for dye removal-a review. *Journal of Environmental Management*, 90, 2313-2342.
- Holmgren, A., Wu, L. & Forsling, W. 1999. Fourier transform infrared and raman study of Alizarin Red S adsorbed at the fluorite water interface. *Spectrochimica Acta Part A*, 55, 1721-1730.
- Jiang, H., Chen, P., Luo, S., Tu, X., Cao, Q. & Shu, M. 2013. Synthesis of novel nanocomposite Fe<sub>3</sub>O<sub>4</sub>/ZrO<sub>2</sub>/chitosan and its application for removal of nitrate and phosphate. *Applied Surface Science*, 284, 942-949.



- Kamarehie, B., Jafari, A., Ghaderpoori, M., Karami, M. A., Mousavi, K. & Ghaderpoury, A. 2018. Data on the Alizarin Red S adsorption from aqueous solutions on PAC, treated PAC, and PAC/gamma approximately  $\text{Fe}_2\text{O}_3$ . *Data in Brief*, 20, 903-908.
- Lemlikchi, W., Sharrock, P., Fiallo, M., Nzihou, A. & Mecherri, M. O. 2014. Hydroxyapatite and Alizarin sulfonate ARS modeling interactions for textile dyes removal from wastewaters. *Procedia Engineering*, 83, 378-385.
- Liang, Y. D., He, Y. J., Zhang, Y. H. & Zhu, Q. Q. 2018. Adsorption property of Alizarin Red S by  $\text{NiFe}_2\text{O}_4$ /polyaniline magnetic composite. *Journal of Environmental Chemical Engineering*, 6, 416-425.
- Liu, M., Zhang, X., Li, Z., Qu, L. & Han, R. 2020. Fabrication of zirconium (IV)-loaded chitosan/ $\text{Fe}_3\text{O}_4$ /graphene oxide for efficient removal of Alizarin Red from aqueous solution. *Carbohydrate Polymers*, 248, 116792.
- Mishra, A. K., Arockiadoss, T. & Ramaprabhu, S. 2010. Study of removal of azo dye by functionalized multi walled carbon nanotubes. *Chemical Engineering Journal*, 162, 1026-1034.
- Monier, M. & Abdel-Latif, D. A. 2012. Preparation of cross-linked magnetic chitosan-phenylthiourea resin for adsorption of Hg(II), Cd(II) and Zn(II) ions from aqueous solutions. *Journal of Hazardous Materials*, 209-210, 240-249
- Moriguchi, T., Yano, K., Nakagawa, S. & Kaji, F. 2003. Elucidation of adsorption mechanism of bone-staining agent Alizarin Red S on hydroxyapatite by FTIR microspectroscopy. *Journal of Colloid and Interface Science*, 260, 19-25.
- Nopkhuntod, S., Dararat, S. & Yimrattanabovorn, J. 2012. Removal of reactive dyes from wastewater by shale. *Songklanakarin Journal of Science and Technology*, 34, 117-123.
- Puchtler, H., Meloan, S. N. & Terry, M. S. 1969. On the history and mechanism of Alizarin and Alizarin Red S stains for calcium. *The Journal of Histochemistry and Cytochemistry*, 17, 110-124.
- Rahbar, N., Jahangiri, A., Boumi, S., Khodayar, M. J. 2014. Mercury removal from aqueous solutions with chitosan-coated magnetite nanoparticles optimized using the box-behnken design. *Jundishapur Journal Natural Pharmaceutical Products*, 9, e15913.
- Rehman, R., Mahmud, T., Anwar, J., Shafique, U., Zaman, W. U. & Ali, F. 2011. Removal of Alizarin Red S (dye) from aqueous media by using alumina as an adsorbent. *Journal-Chemical Society of Pakistan*, Soc. Pak., 33, 228-232.
- Rangabhashyam, S., Anu, N. & Selvaraju, N. 2013. Sequestration of dye from textile industry wastewater using agricultural waste products as adsorbents. *Journal of Environmental Chemical Engineering*, 1, 629-641.
- Salama, A., Shukry, N. & El-Sakhawy, M. 2015. Carboxymethyl cellulose-g-poly (2-(dimethylamino) ethyl methacrylate) hydrogel as adsorbent for dye removal. *International Journal of Biological Macromolecules*, 73, 72-75.
- Shen, C., Shen, Y., Wen, Y., Wang, H. & Liu, W. 2011. Fast and highly efficient removal of dyes under alkaline conditions using magnetic chitosan-Fe(III) hydrogel. *Water Research*, 45, 5200-5210.
- Tan, K. A., Morad, N., Teng, T. T., Norli, I. & Panneerselvam, P. 2012. Removal of cationic dye by magnetic nanoparticle ( $\text{Fe}_3\text{O}_4$ ) impregnated onto activated maize cob powder and kinetic study of dye waste adsorption, *APCBEE Procedia*, 1, 83-89.

- Yang, J. Y., Jiang, X. Y., Jiao, F. P. & Yu, J. G. 2018. The oxygen-rich pentaerythritol modified multi-walled carbon nanotube as an efficient adsorbent for aqueous removal of Alizarin Yellow R and Alizarin Red S. *Applied Surface Science*, 436, 198-206.
- Zhang, Z., Chen, H., Wu, W., Pang, W. & Yan, G. 2019. Efficient removal of Alizarin Red S from aqueous solution by polyethyleneimine functionalized magnetic carbon nanotubes. *Bioresource Technology*, 293, 122100.
- Zolgharnein, J., Asanjrani, N., Bagtash, M. & Azimi, G. 2014. Multi-response optimization using Taguchi design and principle component analysis for removing binary mixture of Alizarin Red and Alizarin Yellow from aqueous solution by nano gamma-alumina. *Spectrochimica Acta. Part A, Molecular and Biomolecular Spectroscopy*, 126, 291-300.



This work is licensed under a [Creative Commons Attribution 4.0 International License](https://creativecommons.org/licenses/by/4.0/).